JNCI J Natl Cancer Inst (2015) 107(4): djv017

doi:10.1093/jnci/djv017
First published online February 20, 2015
Article

ARTICLE

Blockade of MMP14 Activity in Murine Breast Carcinomas: Implications for Macrophages, Vessels, and Radiotherapy

Eleanor I. Ager, Sergey V. Kozin, Nathaniel D. Kirkpatrick, Giorgio Seano, David P. Kodack, Vasileios Askoxylakis, Yuhui Huang, Shom Goel, Matija Snuderl, Alona Muzikansky, Dianne M. Finkelstein, Daniel T. Dransfield, Laetitia Devy, Yves Boucher, Dai Fukumura, Rakesh K. Jain

Affiliations of authors: Edwin L. Steele Laboratory, Department of Radiation Oncology, Massachusetts General Hospital and Harvard Medical School, Boston MA (EIA, SVK, NDK, GS, DPK, VA, YH, SG, MS, YB, DF, RKJ); Department of Surgery (Austin Health), University of Melbourne, Studley Road Heidelberg, VIC, Australia (EIA); Novogen, Hornsby, NSW, Australia (EIA); Novartis Institutes for BioMedical Research, Cambridge, MA (NDK); Centenary Institute of Cancer Medicine and Cell Biology, University of Sydney, Camperdown, NSW, Australia (SG); Department of Biostatistics, Massachusetts General Hospital Biostatistics Center, Boston, Massachusetts (AM, DMF); Department of Pathology, NYU Langone Medical Center and Medical School, New York, NY (MS); Dyax Corp., Burlington, MA (DTD, LD); Departments of Medical Oncology and Cancer Biology, Dana-Farber Cancer Institute, Harvard Medical School, Boston, MA (SG); Tokai Pharmaceuticals, Inc., Cambridge, MA (DTD); Merck Serono S. A., Geneva, Switzerland (LD).

Correspondence to: Rakesh K. Jain, PhD, Edwin L. Steele Laboratory for Tumor Biology, Massachusetts General Hospital, Cox 7, 100 Blossom St, Boston, MA 02114 (e-mail: jain@steele.mgh.harvard.edu) or Dai Fukumura, MD, PhD,dai@steele.mgh.harvard.edu

Abstract

Background: Matrix metalloproteinase (MMP) 14 may mediate tumor progression through vascular and immune-modulatory effects.

Methods: Orthotopic murine breast tumors (4T1 and E0771 with high and low MMP14 expression, respectively; n = 5–10 per group) were treated with an anti-MMP14 inhibitory antibody (DX-2400), IgG control, fractionated radiation therapy, or their combination. We assessed primary tumor growth, transforming growth factor β (TGFβ) and inducible nitric oxide synthase (iNOS) expression, macrophage phenotype, and vascular parameters. A linear mixed model with repeated observations, with Mann-Whitney or analysis of variance with Bonferroni post hoc adjustment, was used to determine statistical significance. All statistical tests were two-sided.

Results: DX-2400 inhibited tumor growth compared with IgG control treatment, increased macrophage numbers, and shifted the macrophage phenotype towards antitumor M1-like. These effects were associated with a reduction in active TGFβ and SMAD2/3 signaling. DX-2400 also transiently increased iNOS expression and tumor perfusion, reduced tissue hypoxia (median % area: control, 20.2%, interquartile range (IQR) = 6.4%-38.9%; DX-2400: 1.2%, IQR = 0.2%-3.2%, $P = .044$), and synergistically enhanced radiation therapy (days to grow to 800 mm^3: control, 12 days, IQR = 9–13 days; DX-2400 plus radiation, 29 days, IQR = 26–30 days, $P < .001$) in the 4T1 model. The selective iNOS inhibitor, 1400W, abolished the effects of DX-2400 on vessel perfusion and radiotherapy. On the other hand, DX-2400 was not capable of inducing iNOS expression or synergizing with radiation in E0771 tumors.

Conclusion: MMP14 blockade decreased immunosuppressive TGFβ, polarized macrophages to an antitumor phenotype, increased iNOS, and improved tumor perfusion, resulting in reduced primary tumor growth and enhanced response to radiation therapy, especially in high MMP14-expressing tumors.

Received: May 20, 2013; **Revised:** April 17, 2014; **Accepted:** January 15, 2015

ARTICLE

Matrix metalloproteinases (MMPs) facilitate cancer progression (1–3). However, broad-spectrum MMP inhibitors failed in part because MMPs mediate both pro- and anticancer effects (4–7) and because off-target, dose-limiting toxicity impeded efficacy (7). To counter these deficiencies, agents targeting specific MMPs have been developed. For breast cancer (BC), MMP14 (membrane type 1-MMP; MT1-MMP) is an especially attractive target (2,8). Genetic knockdown of MMP14 in BC cells impedes their migration and metastases but does not affect their in vitro viability or primary tumor growth (3,8). In contrast, antibody inhibition—which blocks both cancer and stromal MMP14 activity—slows primary tumor growth (9,10). Indeed, a considerable number of reactive stromal cells also express MMP14 (2), illustrating the potential importance of stromal MMP14.

MMP14 facilitates angiogenesis (11–13), and MMP14 blockade can inhibit tumor angiogenesis (9,10). Various antiangiogenic agents, however, can also transiently normalize the tumor vasculature, improving tumor perfusion and oxygenation, leading to enhanced efficacy of chemo- and/or radiation-therapy (14–16). In preclinical models, blockade of MMP14 could enhance the response to cytotoxic therapies (9,10). These findings prompted us to determine a potential improvement in tumor vascular function by MMP14 blockade.

The antiangiogenic effect of MMP14 inhibition is thought to result from reduced activation of MMP2 by MMP14 (9). However, other MMP14 targets have not been studied, including transforming growth factor β (TGFβ), a mediator of vascular response and a potent immunosuppressor. TGFβ is associated with poor clinical outcome in BC (17). TGFβ has proangiogenic activities and mediates vessel stabilization (18–20). TGFβ inhibitors increase antitumor immunity associated with increasing interferon (IFN)-γ and granzyme B production from natural killer (NK) cells and cytotoxic $CD8^+$ T cells, reducing T regulatory cells, and shifting macrophages toward an inducible nitric oxide synthase (iNOS)–expressing antitumor M1-like phenotype and away from tumor-supportive M2-type (21–27).

In this study we investigated if DX-2400 (9), a highly selective MMP14 inhibitory antibody, could decrease TGFβ levels and alter the macrophage phenotype in tumors. We also aimed to determine if DX-2400 could improve tumor vessel function and thus provide additional benefits when combined with radiation therapy.

Methods

Tumor Models

All animal procedures followed Public Health Service Policy on Humane Care of Laboratory Animals guidelines and were approved by the Massachusetts General Hospital Institutional Animal Care and Use Committee. A single 4T1 primary tumor per mouse was established by implanting $1x10^5$ cells into the third mammary fat pad (MFP). As previous studies using anti-MMP14 antibodies employed NU/NU (nude) mice (9,10), we also used female (age six to eight weeks) nude mice to assess if macrophages were capable of responding to DX-2400 in the absence of adaptive immunity. We then confirmed key findings in immunocompetent C57BL/6 mice bearing syngenic E0771 tumors. E0771 tumors were established by implanting $2x10^5$ cells in the MFP of wild-type C57BL/6 or *NOS2*$^{-/-}$ mice. For optical frequency domain imaging, an MFP window was fitted around 4T1 tumors of approximately 10 mm^3 in syngenic BALB/c mice age 10 to 12 weeks. Details are provided in Supplementary Methods (available online).

Treatments

Treatment began once primary tumors reached approximately 40 mm^3. Control IgG or DX-2400 was injected at an established effective dose (10 mg/kg) every 48 hours i.p. (9). Treatment continued for a maximum of 10 injections. Local radiotherapy began four days after tumors reached approximately 40 mm^3 (ie, equivalent to day 4 of DX-2400 or IgG treatment). Fractionated irradiation was given using XRAD 320 irradiator (Precision X-Ray, Inc.) at 3.5 Gy/min to a total dose of 6 Gy per daily fraction on three consecutive days. A selective iNOS inhibitor (1400W dihydrochloride, Enzo Life Sciences) was delivered by s.c. osmotic minipump (Alzet 1002; 0.42 mg/kg/hour).

Immunostaining

Details are provided in the Supplementary Methods (available online). Primary antibodies included: MMP14, cluster differentiation factor 31 (CD31, endothelial cell marker), NG2 (pericyte marker), Collagen IV (basement membrane (BM) marker), iNOS-FITC, CA9 (hypoxia marker), HSP90, SMAD2/3, F4/80-Cy5 (macrophage marker), mannose receptor C type 1 (MRC1, M2 marker), granzyme B (cytotoxic activity marker), NK1.1-Cy3 (NK cell marker), proliferating cell nuclear antigen (PCNA, proliferation marker), and Apoptag (apoptosis marker).

Optical Frequency-Domain Imaging

Optical Frequency-Domain Imaging (OFDI) allows detailed analysis of the geometry and functionality of the perfused tumor vasculature (28). OFDI was performed at day 4 using a custom-built microscope as described previously (28). Additional details are provided in the Supplementary Methods (available online).

Western Blotting and Antibody Array

Details are provided in the Supplementary Methods (available online). Protein was collected from tumors following six days of treatment. Primary antibodies included MMP14 (Abcam, ab51074, 1:1000), iNOS (BD Biosciences, 610329, 1:500), TGFβ (Cell Signaling, 3711S, 1:1000), and β-actin (Sigma, A5441, 1:5000). The antibody array (RayBiotech, AAM-INF-1) protocol followed manufacturer's instructions.

Image Analysis

Details are provided in the Supplementary Methods (available online). Quantification of staining was performed using an in-house MATLAB (MathWorks) segmentation algorithm or ImageJ (29). Relative densitometry was determined using ImageJ with normalization to the loading control.

Statistical Methods

PRISM (GraphPad Software, version 6e) and Statistical Analysis System (SAS) 9.4 were used for analyses. All statistical analyses between two groups were performed using the nonparametric Mann-Whitney test. However, when more than two groups were assessed, following confirmation that normality was achieved (using Kolmogorov-Smirnov test in PRISM), data were assessed by analysis of variance (ANOVA) followed

by Bonferroni adjusted post hoc *t* tests for multiple pairs of interest without a priori selection. Robust regression and outlier removal (ROUT, GraphPad) was used to determine if outliers were present. All statistical tests were two-sided. A mixed model was fitted to test the differences between treatment and control tumor growth curves accounting for repeated measurements over time and mouse as a random effect. Differences were considered statistically significant at *P* values of less than .05; *P* values between .05 and .1 were considered to show a trend and are also presented in figures. Data are presented as median with the interquartile range and, in the case of boxplots and column graphs, maximum and minimum values.

Results

MMP14 Expression in Murine BC Models

We determined MMP14 protein expression in 4T1 and E0771 BC cells in in vitro culture and in tumor tissues in vivo (Figure 1A). Although MMP14 protein was detected in both BC models, 4T1 tumors express a notably higher level of MMP14 compared with E0771. We confirmed that MMP14 was membrane associated in these models (Figure 1B). We then costained for MMP14 and F4/80 and discovered that essentially every macrophage expressed MMP14 (Figure 1, C and D), thus showing that MMP14 may not be differentially expressed by M1- and M2-type macrophages.

Efficacy of anti-MMP14 antibody (DX-2400) in vivo and in vitro. We confirmed that DX-2400 treatment reduced collagenolytic activity, a readout of MMP14 activity, in 4T1 tumors effectively in vivo (*P* = .0457) (Figure 1, E and F). We also confirmed that DX-2400 treatment of 4T1 cells in vitro did not affect cell viability (Figure 1G), but it statistically significantly inhibited cell invasion through a collagen matrix in a dose-dependent manner (*P* = .0314 with DX-2400 at 0.2 µg/mL to *P* = .0004 following DX-2400 at 100 µg/mL treatment) (Figure 1H).

Effect of Anti-MMP14 Treatment on BC Growth

Monotherapy with the anti-MMP14 antibody (DX-2400) statistically significantly delayed both 4T1 and E0771 tumor growth. A mixed model indicated a statistically significant reduction in tumor growth rate following DX-2400 treatment in both tumor models (*P* < .001 for both models) (Figure 2, A and B; Supplementary Figure 1, A and B, available online). Subsequent analysis of each individual time point indicated that this divergence in tumor growth was statistically significant from day 6 onwards (4T1, *P* = .0028, CT 279.9 mm^3 ± 117.7, DX 128.4 mm^3 ± 51.2; E0771, *P* = .017, CT 144.9 mm^3 ± 57.4, DX 78.14 mm^3 ± 46.5; mean ± SD). Consistent with reduced 4T1 growth, there was a trend for increased apoptosis at day 4 and necrosis at day 10 (*P* = .0606 and *P* = .0590) (Figure 2, C and D; Supplementary Figure 2, A and B, available online). Although apoptosis at day 4 was not statistically significantly reduced, zero out of five control IgG–treated tumors were found to have a high frequency of apoptosis (Figure 2C) while four out of six DX-2400–treated tumors had areas of high apoptotic rates. Thus, the lack of significance could reflect the small sample size. Proliferation was statistically significantly inhibited at day 4 (*P* = .0411, CT 1113 proliferative cells/FoV [interquartile range {IQR} = 973–1182], DX 908 [IQR = 686–988], median [lower quartiles to higher quartiles]) with a trend towards decreased proliferation at day 10 (*P* = .093) (Figure 2, E and F; Supplementary Figure 2, C and D, available online).

Effect of MMP14 Blockade on Tumor-Associated Macrophages

Given the early (day 4) reduction in proliferation and subsequent tumor growth delay, we aimed to determine if the tumor microenvironment was also altered by treatment at this stage. In 4T1 BC, DX-2400 led to a modest increase in F4/80$^+$ cell numbers at day 4 (*P* = .0148, CT 0.100 staining area/DAPI area [IQR = 0.03–0.27], DX 0.339 [IQR = 0.23–0.45]) and a dramatic increase in the proportion of macrophages expressing iNOS (an M1 marker) (*P* = .0003, CT 0.004 area colocalization [IQR = 0.001–0.005], DX 0.140 [IQR = 0.066–0.256]) (Figure 3, A and B). We also examined markers of cytotoxic activity (granzyme B) and M2 phenotype (MRC1). Granzyme B, typically expressed by NK cells in nude mice, was substantially increased by DX-2400 (*P* = .0012, CT 0.006 staining area/DAPI area [IQR = 0.0008–0.0316], DX 0.087 [IQR = 0.0374–0.1456]) (Figure 3C). Some macrophages also expressed granzyme B, and this was higher in DX-2400–treated tumors (*P* = .0005) (Supplementary Figure 3, A-C, available online). Moreover, we found that granzyme B–positive cells associated more frequently with F4/80$^+$ cells in DX-2400–treated tumors (*P* = .0005) (Supplementary Figure 3, A and D). In contrast to M1-type markers, DX-2400 reduced MRC1 positivity (*P* = .0111, CT 0.008 area colocalization [IQR = 0.007–0.025], DX 0.003 [IQR = 0.0008–0.0065]) (Figure 3D). We also found that active TGFβ and its downstream signaling partner SMAD2/3 were reduced in 4T1 tumors by DX-2400 treatment (*P* = .0011) (Figure 3, F and G). In vitro, we saw that macrophages treated with TGFβ decreased expression of the M1 marker iNOS (Supplementary Figure 4A, available online). Supporting a shift in macrophage response, we used an antibody array to provide an indication of the broader cytokine profile of tumors. We found that IFNγ and GM-CSF (M1 associated cytokines) were generally higher in DX-2400–treated tumors, while interleukin (IL)-4, IL-10, and G-CSF (M2-type responses) were generally lower following DX-2400 treatment (Supplementary Figure 4B, available online). Furthermore, NK cell numbers increased with DX-2400 in 4T1 tumors (Supplementary Figure 4, C and D). Statistically significant changes were also seen in E0771 tumors, such as the increase in F4/80$^+$ (*P* = .0260, CT 0.064 staining/DAPI [IQR = 0.04–0.13], DX 0.171 [IQR = 0.11–0.26]) (Figure 3H) and iNOS$^+$F4/80$^+$ (*P* = .0022, CT 0.005 area colocalization [IQR = 0.0005–0.0133], DX 0.047 [IQR = 0.022–0.068]) (Figure 3I), as well as granzyme B+ cells, NK cells, and granzyme B+ NK cells (Supplementary Figure 4, E-I, available online). Similarly, the proportion of M1-type macrophages increased in DX-2400–treated 4T1 tumors grown in syngeneic BALB/c mice (Supplementary Figure 4J, available online). Collectively, we found that MMP14 blockade shifts immune cell and cytokine profiles from immunosuppressive to antitumor phenotype in our BC models.

Effect of MMP14 Inhibition on BC iNOS Expression

While assessing iNOS as an M1 marker, we also noted a statistically significant increase in gross tumor-associated iNOS in the 4T1 tumors following DX-2400 treatment (*P* = .0095, CT 0.005 staining/DAPI [IQR = 0.002–0.008], DX 0.013 [IQR = 0.007–0.019]) (Figure 4A-C; Supplementary Figure 5A, available online). On the other hand, baseline iNOS was approximately seven-fold higher in the E0771 model compared with the 4T1 model (CT 0.028 staining/DAPI [IQR = 0.012–0.061], DX 0.057 [IQR = 0.026–0.153]) (Figure 4, C and D; Supplementary Figure 6, available online), which may have limited the ability of DX-2400 to further increase iNOS levels in this tumor model. In 4T1 tumors, we also found

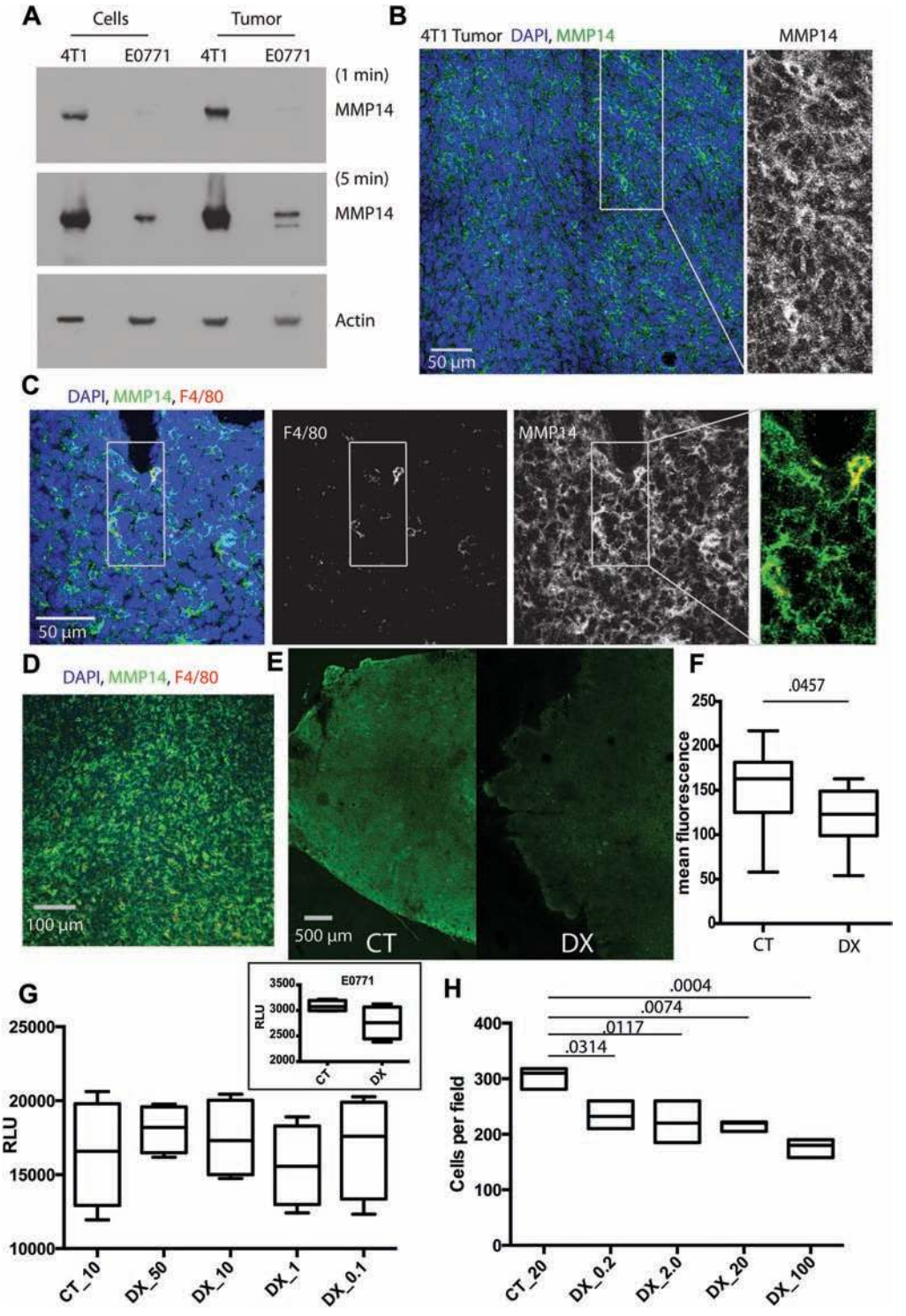

Figure 1. MMP14 expression and activity in breast cancer in vivo and its direct effects on tumor cells in vitro. **A)** Western blot of MMP14 in 4T1 and E0771 cell lines and tumors grown orthotopically in the mammary fat pad of nude or C57BL6 mice, respectively. Blots exposed for one minute or five minutes for MMP14 and one minute for β-actin. **B-D)** Immunofluorescence staining for MMP14 in 4T1 tumors. MMP14 was broadly expressed within the tumor (**B**) and showed bright staining on macrophages (F4/80 marker) (**C-D**). All macrophages appeared to express MMP14; ie, no red single staining cells, only yellow colocalization visible (**C**, higher magnification; **D**, lower magnification). **E-F)** Collagenolytic activity decreased following treatment with DX-2400 (10 mg/kg). Representative DQ-collagen type I images; control (**E**) and quantification (relative fluorescence units) of collagenolytic activity (DQ-collagen type-I) (**F**). **G)** Data from five replicates are shown. The effect of DX-2400 concentration (µg/mL) on 4T1 cell viability (inset, E0771 cells treated with 50 µM DX-2400) expressed as relative luminescence units. BC cell viability was unaffected by DX-2400 at the concentrations of 0.1–50 µg/mL. E0771 cell data in the inset was $P = 0.1$. Here, day 3 data are presented. Day 1 and 2 data were similar. **H)** Data from three replicates are shown. The effect of DX-2400 concentration (µg/mL) on 4T1 cell invasion. In contrast to cell viability, cell invasion through collagen I was statistically significantly reduced by DX-2400 at all concentrations tested (0.2–100 µg/mL). **F-H)** Data are presented as median with the interquartile range (**box and whiskers**). *P* values are shown. Analysis of invasion and viability were performed in triplicate, $n > 7$ for DQ collagen analysis. Statistical significance determined by two-sided Mann-Whitney test for DQ analysis and analysis of variance with Tukey's correction. CT = control; DX = DX-2400; RLU = relative luminescence unit.

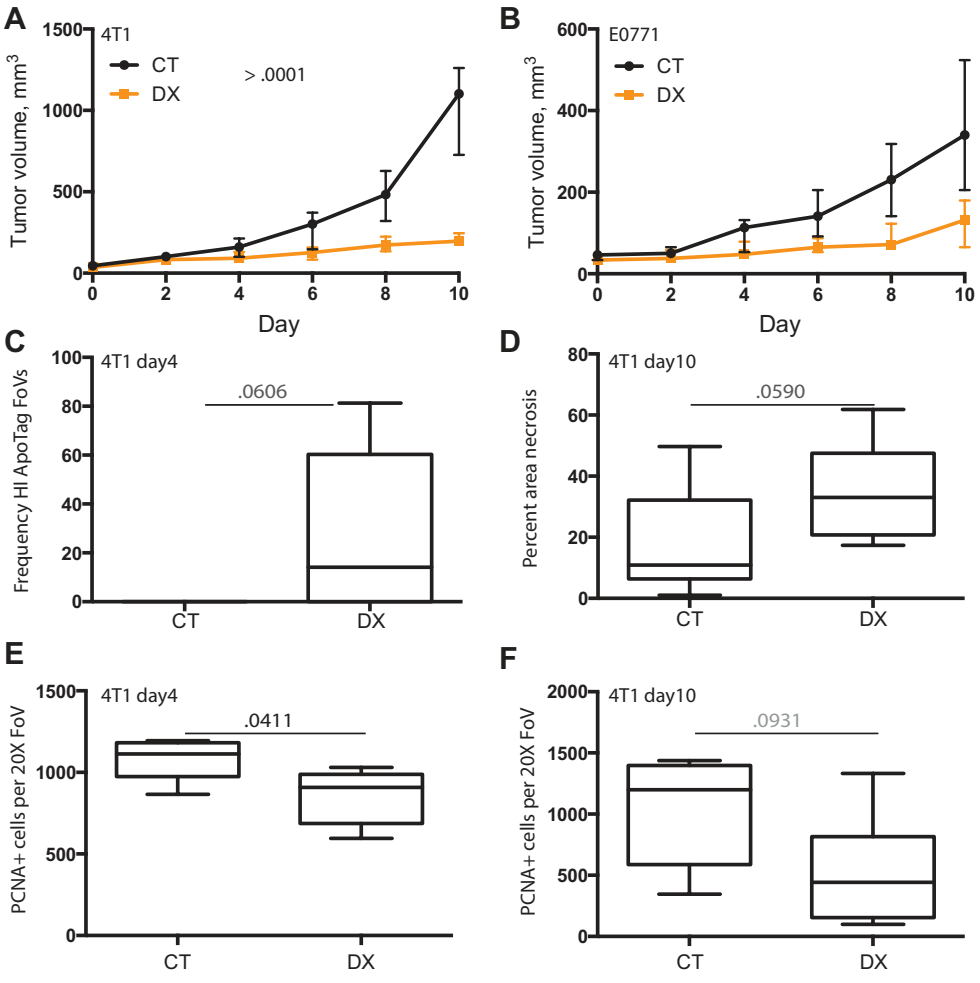

Figure 2. Inhibition of 4T1 and E0771 tumor growth by MMP14 blockade. Mice were treated with control IgG (CT) or DX-2400 (DX) (10 mg/kg every 48 hours, up to 10 injections) once tumors reached approximately 40 mm^3 (day 0) to day 10, at which time mice were killed. **A-B)** Tumor growth curves. Data for 4T1 in nude (**A**) and E0771 in C57BL6 (**B**) are presented as median and interquartile range. Individual tumor growth curves are provided in Supplementary Figure 1 (available online). Tumor growth rates were statistically significantly different according to a mixed model analysis. **C-D)** Cell death. There was a trend towards increased apoptosis with DX-2400 treatment at day 4 (**C**; high-frequency Apoptag staining assessed as greater than 10 apoptotic cells per field of view) and, similarly, necrosis tended to be greater in day 10 samples from DX-2400 treated animals. **E-F)** Cell proliferation. Day 4 proliferation (proliferating cell nuclear antigen) was decreased by DX-2400 (**E**), while day 10 proliferation showed a trend (**F**). Images of Apoptag, necrosis, and PCNA are provided in Supplementary Figure 2 (available online). All data from panels **C** to **F** were obtained from 4T1 tumors in nude mice. Data are presented as median with the interquartile range (**box**) and maximum and minimum values (**whiskers**) for panels **C** to **F**. *P* values determined by two-sided Mann-Whitney test. Samples sizes: n = 6 for all analyses except day 10 necrosis (n > 8) and tumor growth curves (n = 10 for 4T1 and n = 7 for E0771). CT = control; DX = DX-2400; FoV = field of view; HI = high-frequency; PCNA = proliferating cell nuclear antigen.

a statistically significant increase in the colocalization of HSP90 (normally degraded by MMP2 [30]) with iNOS in DX-2400–treated tumors at day 4 (CT 0.11 colocalization area [IQR = 0.03-0.024], DX 0.31 [IQR = 0.19–0.49], *P* = .0205) (Figure 4, E and F). HSP90 is an enhancer and essential cofactor of iNOS (31,32) and presumably facilitates increased iNOS levels in 4T1. Moreover, the increase in IFNγ seen in the antibody array could also increase tumor iNOS expression (33,34).

Effect of Anti-MMP14 Antibody Treatment on Tumor Vasculature

To investigate DX-2400–associated changes in the tumor vascular geometry and function, we used a robust noninvasive imaging technique, OFDI, which specifically visualizes perfused (containing moving red blood cells) vessels. We found a statistically significant increase in the total number of perfused vessels with DX-2400 treatment (*P* = .0205, CT 73 vessels/volume [IQR = 60–155], DX 196 [IQR = 165–385]) (Figure 5, A and B; Supplementary Figure 7, available online). Reasoning that NO is a vasodilator (35,36), we assessed vessel diameter. We confirmed fewer small-diameter vessels (less than 15 μm) in DX-2400–treated 4T1 tumors (*P* = .0210) (Figure 5C). Additionally, DX-2400 reduced the maximum tortuosity of vessels (*P* = .0460, CT 30 tortuosity index [IQR = 12–46], DX 10 [IQR = 6–12]) (Figure 5D). Histological analyses of tumors collected after four to 10 days of treatment revealed no notable change in vessel (CD31) staining, while vessel maturity (pericyte coverage) was improved in 4T1 tumors, although only on day 10 (Supplementary Figure 8, available online). These results suggest that the antiangiogenic effects of MMP14 inhibition shown by others (9,10) may occur only after extended treatment, with higher doses (30 mg/kg Devy et al. (9) compared with 10 mg/kg used here), or are model specific. This is also consistent with previous findings that the dose of anti-VEGFR2 treatment induces different effects on vasculature (37). We also assessed functionality of these vessels in tissue sections

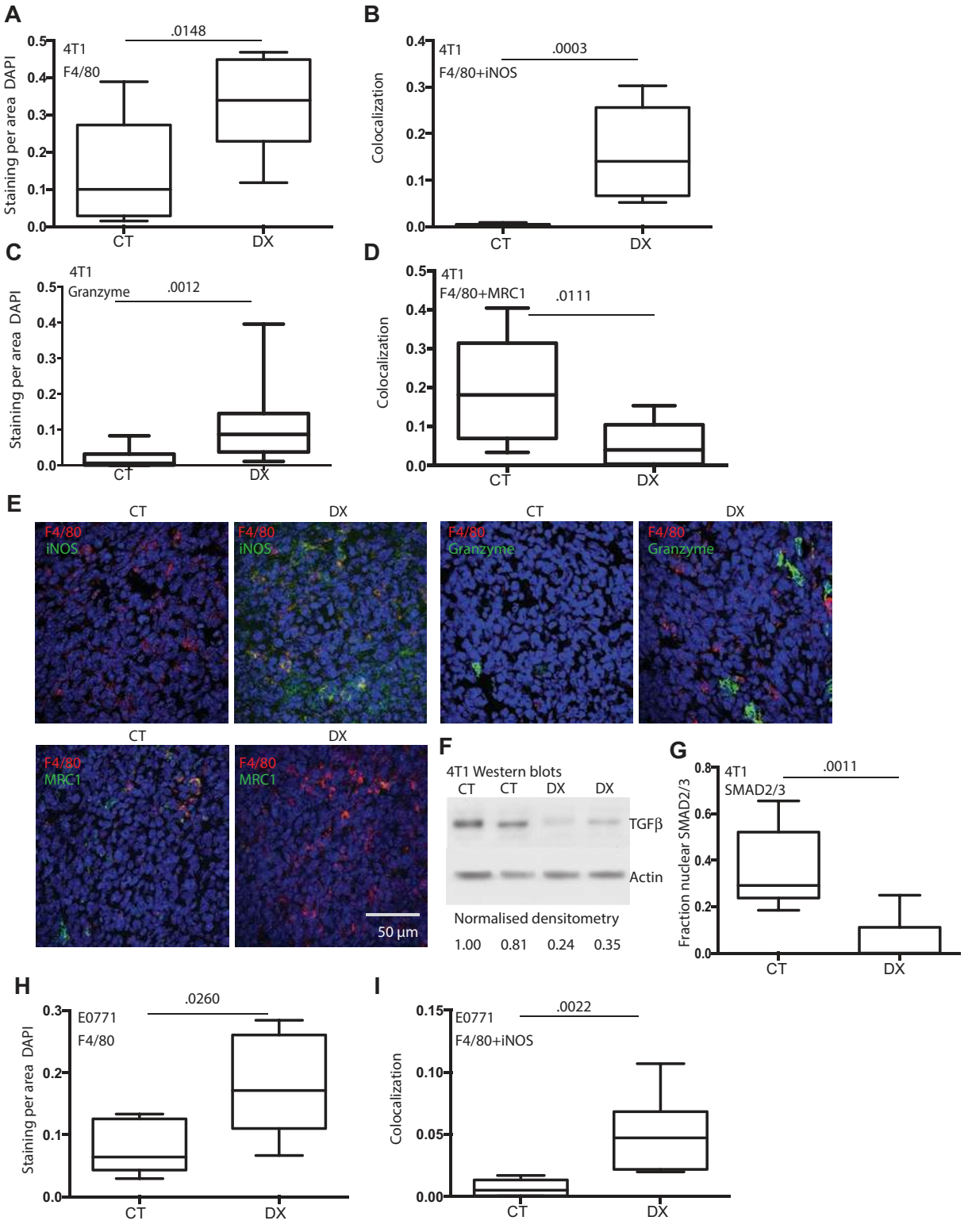

Figure 3. Effect of anti-MMP14 treatment on F4/80⁺ macrophages and M1-like state. **A-G)** Data and representative images from day 4 4T1 tumors in nude mice except western blot of TGFβ (**F**, day 6). Both total F4/80⁺ area (**A**) and the area costaining with iNOS (an M1 marker) (**B**) were increased by DX-2400 (DX) treatment compared with control (CT). Granzyme B (cytotoxic activity) also increased with treatment (**C**), while MRC1 (an M2 marker) (**D**) decreased following DX-2400 treatment. **E)** Representative images of stains. The stain performed is indicated at the **top left** of each CT image with the matched DX to the **right**. A **scale bar** is presented on the **bottom right** and is the same for all images (50 µm). **F)** A Western blot confirmed a decrease in active TGFβ (molecular weight ~25 KDa). **G)** DX decreased nuclear localization of SMAD2/3, downstream of TGFβ activation. **H-I)** Data from day 4 E0771 tumors in C57BL6 mice. An increase in total macrophages (**H**) and iNOS-expressing M1 macrophages (**I**) for E0771 tumors confirmed results from the 4T1 model. Data are presented as median with the interquartile range (**box**) and maximum and minimum values (**whiskers**). Statistical significance determined by two-sided Mann-Whitney test; n = 8 for all analysis of 4T1 samples, and n = 6 for E0771 samples. Additional associated images and data are provided in Supplementary Figures 3 and 4 (available online). CT = control; DX = DX-2400.

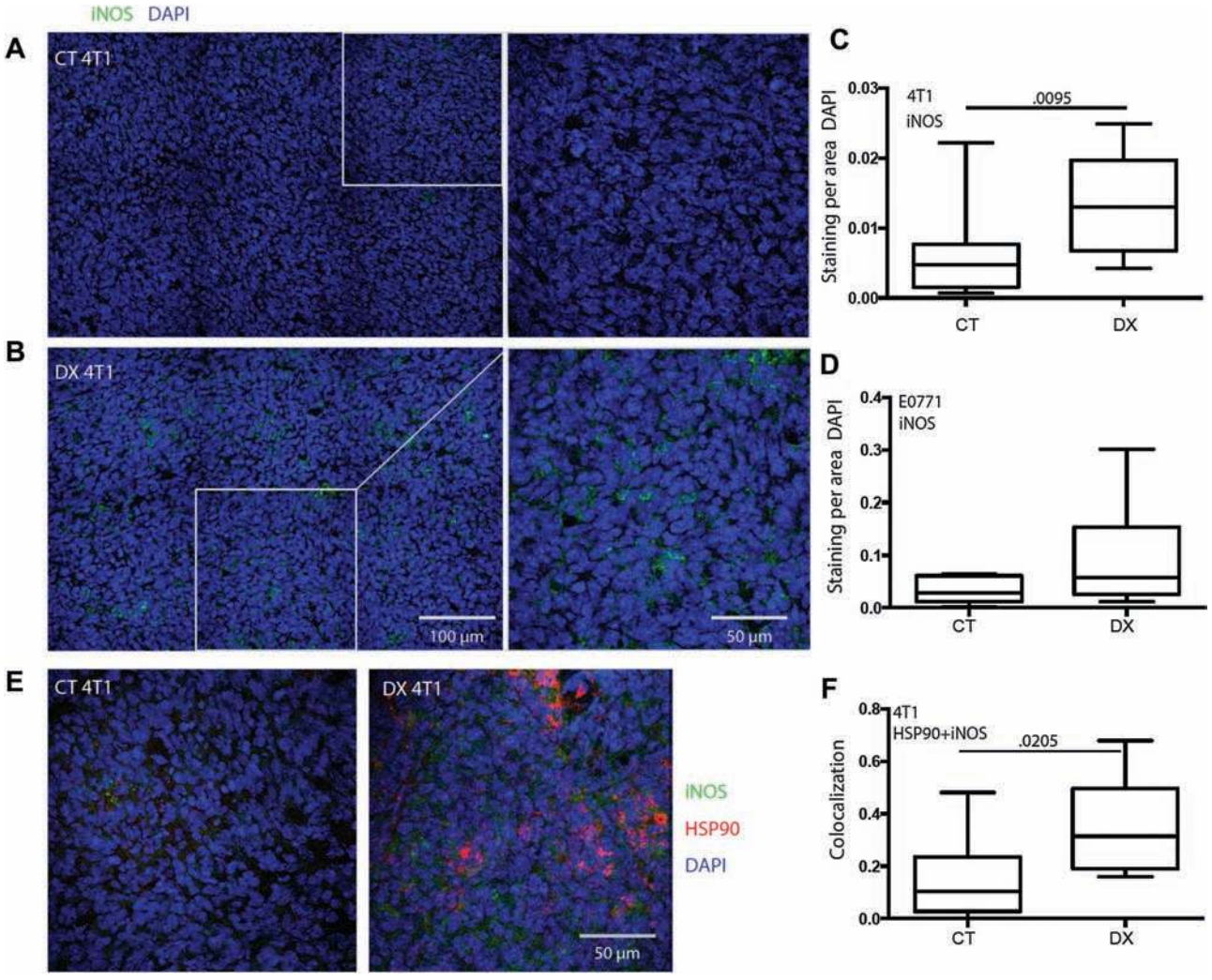

Figure 4. Effect of MMP14 inhibition on iNOS expression in 4T1 tumors. **A-C)** Immunofluorescence staining of iNOS in 4T1 (**A & B,** representative images of control [CT] and DX-2400 [DX] treatment, respectively) revealed an increase with DX-2400 treatment at day 4 in 4T1 tumors (**B**). iNOS levels were not statistically significantly changed by DX-2400 treatment in the E0771 tumor model (**D**). **E-F)** HSP90 and iNOS expression. **E)** Representative images of HSP90 and iNOS immunofluorescent stains). HSP90, an essential cofactor and activator of iNOS, colocalization with iNOS also statistically significantly increased in the 4T1 tumor model (**F**). **Scale bars** are presented in the **bottom right** of each DX image and are the same for CT and DX images. Data are presented as median with the interquartile range (**box**) and maximum and minimum values (**whiskers**); n = 6 for E0771 samples, and n = 10 for 4T1 iNOS analysis, and n = 7 for HSP90+iNOS analysis. Statistical significance determined by two-sided Mann-Whitney test. Additional associated images and data are provided in Supplementary Figures 5 and 6 (available online). Note: y-axis scales in panels **A** and **C** are optimized for each tumor model. CT = control; DX = DX-2400.

using trichrome staining ($P = .0218$, CT 0.6 perfused vessels/field of view [IQR = 0.42–0.67], DX 2.2 [IQR = 1.8–3]) (Figure 5E) and a vessel tracer Hoechst (Supplementary Figure 9, available online) and confirmed the OFDI findings—increased perfusion with DX-2400 treatment. Further, hypoxia, assessed by CA9 staining was also reduced by DX-2400 in 4T1 tumors (median % area: control, 20.2% [IQR = 6.4%-38.9%]; DX-2400: 1.2% [IQR = 0.2%-3.2%], $P = .044$) (Figure 5F; Supplementary Figure 10, available online). NO, a potent vasodilator, is an important regulator of vessel function (38). The increase in vessel diameter without changes in the number of endothelial cells (CD31 positivity) suggests that functional vessel dilatation rather than hyper proliferation plays a key role in vessel diameter increase in this setting. Indeed, blockade of iNOS (by 1400W) prevented the DX-2400–induced improvement in perfusion and oxygenation (Figure 5, E and F). In E0771 tumors there was no statistically significant difference in hypoxia between DX-2400 and control (Figure 5G), possibly reflecting the lack of increased tumor iNOS in this model.

Effect of MMP14 Blockade and Radiation Combined Treatment

Radiation therapy, similar to DX-2400, delayed 4T1 tumor growth compared with control (days to grow to 800 mm^3: control, 12 days [IQR = 9–13 days]; DX, 19 days [IQR = 18–20 days]; R, 17.5 days [IQR = 16–20 days]; and DXRDX, 29 days [IQR = 26–30 days], $P \leq .001$) (Figure 6, A and B; Supplementary Figure 11A, available online). The combination therapy resulted in superior growth inhibition compared with either monotherapy ($P \leq .0001$), and this effect was greater than the expected additive effect ($P = .054$, and, confirmed in Figure 6F, $P = .042$), demonstrating synergy between these therapies. In E0771 tumors, identical radiation and DX-2400 treatments were also effective, but their combination led to an additive tumor growth delay only ($P = .430$) (Figure 6, C and D; Supplementary Figure 11B, available online).

To understand when DX-2400 and irradiation treatments interact and if this correlated with day 4 changes in tumor perfusion

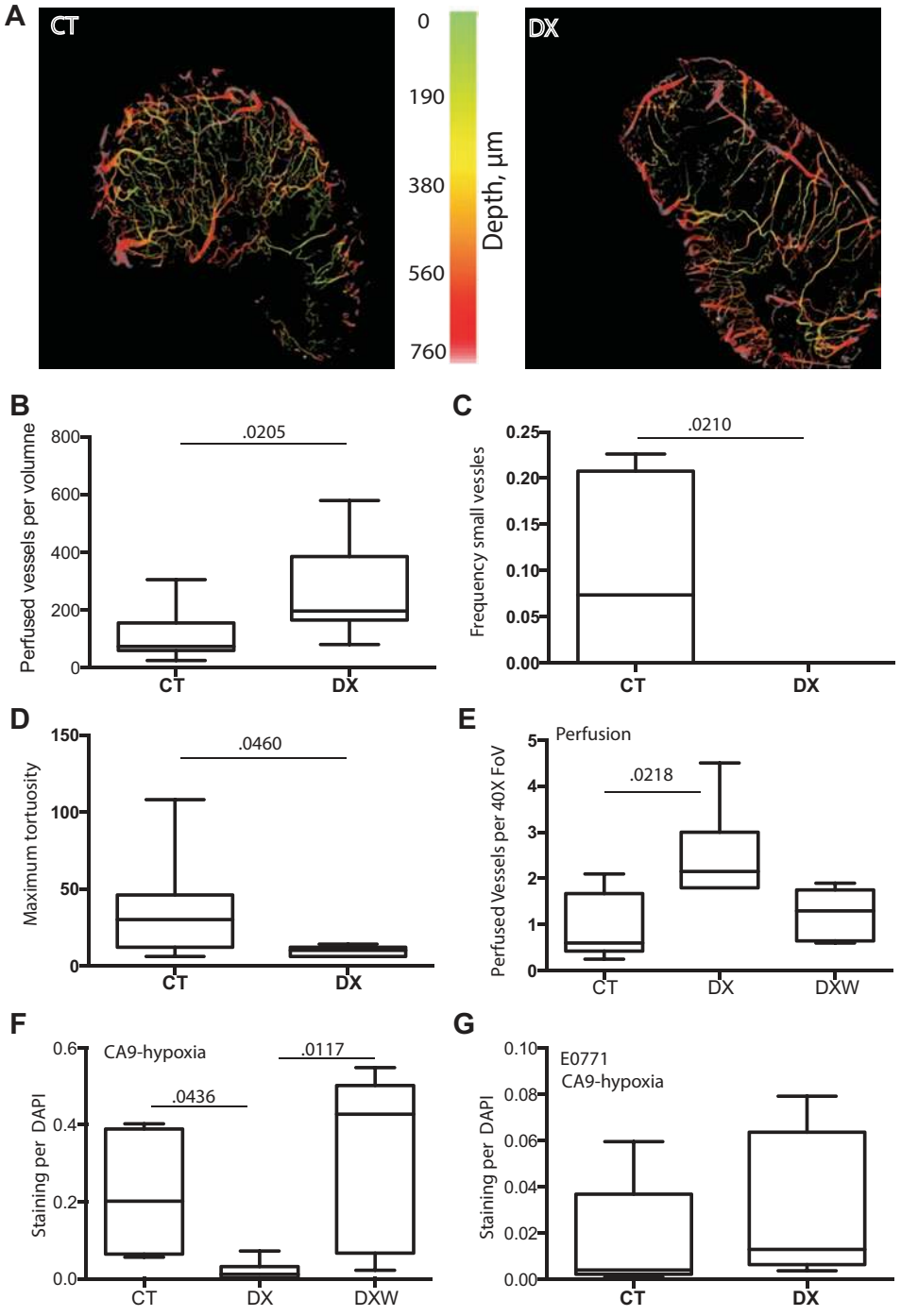

Figure 5. Effect of DX-2400 and iNOS blockade on perfusion and hypoxia in the 4T1 tumor model. **A)** Representative optical frequency domain images (OFDI) of control (CT)- and DX-2400 (DX)–treated tumors. **B-E)** Analyses of vascular parameters. The number of perfused vessels was increased by DX-2400 (**B**), while the frequency of vessels with a diameter of less than 15 µm was decreased by DX-2400 (**C**). The maximum tortuosity of vessels was also decreased by DX-2400 (**D**). Perfusion, assessed on trichrome stained tumor sections, was confirmed to increase with DX-2400 treatment, while blockade of iNOS with 1400W (DXW) prevented the DX-2400–associated increase in perfusion (**E**). **F-G)** Assessment of hypoxia. DX-2400 alone was also seen to decrease staining of CA9 (a marker of hypoxia), while the addition of 1400W to DX-2400 prevented this decrease (**F**). Contrary to the 4T1 model (**A-F**), the E0771 tumor model did not show a decrease in hypoxia with DX-2400 treatment (**G**). All data are from day 4 after treatment initiation. Data are presented as median with the interquartile range (**box**) and maximum and minimum values (**whiskers**). Sample size: n = 7 for OFDI analyses, n = 5 or 6 for all other analyses (ie, panels **E-G**). *P* values determined by two-sided Mann-Whitney test for **B-D** and **G** and by Kruskal-Wallis test for **E** and **H**. Additional associated images and data are provided in Supplementary Figures 7–10 (available online). Note: y-axis scales in panels **F** and **G** are optimized for each tumor model. CT = control; DX = DX-2400; DXW = 1400W in addition to DX; FoV = field of view.

and oxygenation, we compared the efficacies of three combination strategies: 1) as above, 10 DX-2400 injections over 20 days before, during, and after irradiation (DXRDX), 2) three antibody injections beginning at day 0 and extending to day 4 when the first fraction of irradiation was given (DX_R), or 3) seven postirradiation injections (R_DX). Pretreatment with DX-2400 essentially replicated the benefit seen in the DXRDX group (Figure 6E; Supplementary Figure 11C, available online). In contrast, the

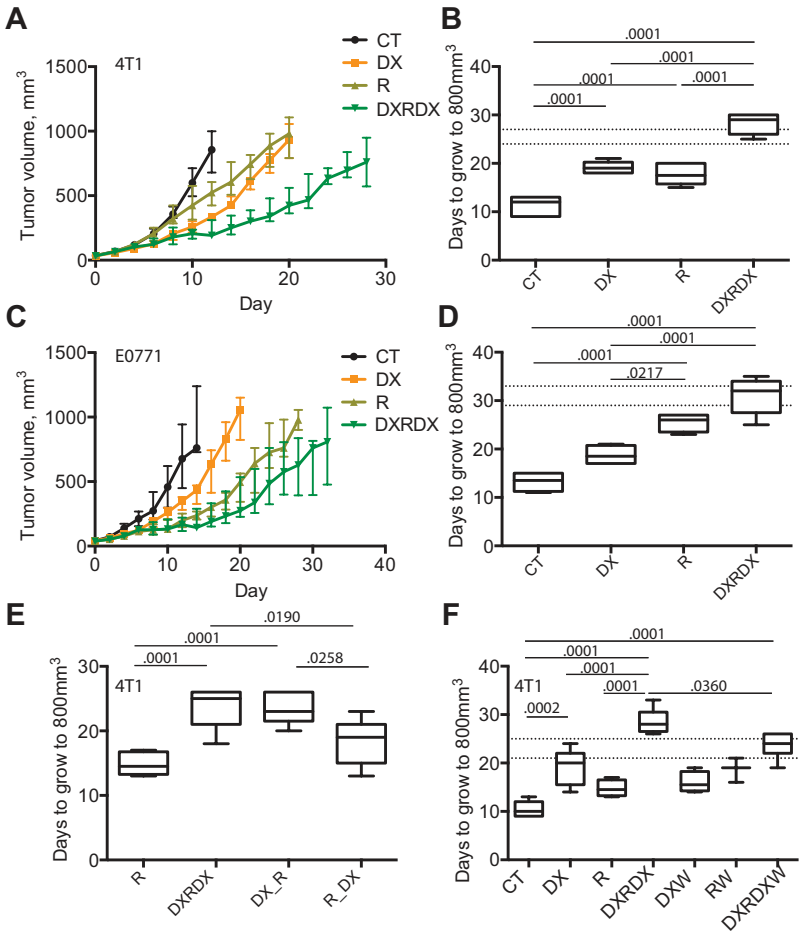

Figure 6. The effect of anti-MMP14, radiation, and their combination on BC models. **A-D)** The combination of DX-2400 and radiation is modestly synergistic in the 4T1 tumor model and additive in the E0771 tumor model. Tumor growth curves for 4T1 tumors (**A**) and E0771tumors (**C**) in mice treated with control (CT), DX-2400 (DX), local fractionated irradiation (R; days 4, 5, and 6), or their combination (DXRDX). Mice were maintained and tumors measured until tumors reached approximately 1000 mm^3 or until morbidity was evident. Data are presented as median and interquartile range (panels **A** and **C**) with individual curves presented in Supplementary Figure 11 (available online). All other data are presented as median with the interquartile range (**box**) and maximum and minimum values (**whiskers**). Sample size: n = 6 for 4T1 and n = 4 or 5 for E0771. The time (days) taken for tumors to grow to 800 mm^3 was used to assess tumor growth delay (panels **B**, 4T1, and **D**, E0771). The combination of DX-2400 and radiation was synergistic in the 4T1 model (**B**; expected additive range of DX+R is shown as **horizontal dashed lines**), while the combination was additive in the E0771 model (**D**). **E)** The effects of the timing of MMP14 inhibition. Ten DX-2400 injections (DXRDX) compared with three initial injections of DX-2400 (DXR; DX on days 0, 2, and 4 with radiation on days 4, 5, and 6) and seven postirradiation injections (RDX). **F)** The effects of iNOS were assessed using 1400W in addition to DX (DXW), radiation (RW), and the combination (DXRDXW). The synergy associated with combination treatment in the 4T1 model was lost when iNOS was inhibited. Analysis of variance with Bonferroni post hoc t test was performed for analysis of tumor growth. All statistical tests were two-sided. Additional data are provided in Supplementary Figure 11 (available online). CT = control; DX = DX-2400; DXR = three initial injections of DX-2400 plus radiation; DXRDX = ten DX-2400 injections plus radiation; DXRDXW = combination DXRDX plus 1400W; DXW = DX-2400 plus 1400W; RDX = radiation followed by DX-2400; RW = radiation plus 1400W.

postirradiation treatment protocol did not result in a statistically significant tumor growth delay compared with irradiation alone and was statistically significantly worse (P = .026, R 14.5 days [IQR = 13–17], DXRDX 25 [IQR = 21–26], DX_R 23 [IQR = 21.5–26], and R_DX 19 [IQR = 15–21]) than the standard combination. Thus, the relatively short "priming" of tumors by DX-2400 treatment before irradiation appears critical for their synergism.

Blockade of iNOS by 1400W in 4T1 tumors (Figure 6F) or 1400W or genetic knockout in *NOS2*$^{-/-}$ mice in E0771 tumors did not alter the efficacy of DX-2400 monotherapy (Supplementary Figure 11, E and F, available online), suggesting that iNOS and presumably its effects on vessels do not contribute to the tumor growth delay induced by DX-2400 alone. However, the addition of 1400W to the combined DX-2400–radiation therapy was associated with a stimulation of tumor growth, ie, a loss of efficacy and synergy, compared with this combined therapy alone (P = 0.036, RDX 28 [IQR = 26.5–30.5], RDXW 24 [IQR = 22–26]) (Figure 6F; Supplementary Figure 11D, available online), suggesting that iNOS contributes to the tumor growth delay benefit of adding radiation to DX-2400. These findings are consistent with the abrogation by 1400W of effects of DX-2400 on tumor perfusion and oxygenation (Figure 5, E and F).

The P values presented in Figure 6 were determined using ANOVA with Bonferroni adjustment (as the variables of interest fit the required normality assumption). It is worth noting that a Kruskal-Wallis analysis confirmed key findings: statistically significant reduction in tumor growth with DX-2400 (in the 4T1 model; P = .0243), statistically significant reduction in tumor growth upon combination treatment (in both models; 4T1 P < .0001, E0771 P = .0012), a statistically significant reduction in tumor growth compared with radiation alone only when DX-2400 was given before/during radiation (P = .0051 and .0037, respectively) but not after radiation (P = .8865), and reduced efficacy of the combination therapy when iNOS was blocked (tumor growth

reduction compared with control; $P = .0001$ for RDX compared with $P = .0012$ for RDXW).

Discussion

Here, we show that the treatment with highly selective MMP14 inhibitory antibody, DX-2400, was associated with the decrease in active TGFβ—an immunosuppressive cytokine—in murine BC tissue. Consistent with this, macrophages were shifted towards antitumor phenotype. Furthermore, we found that DX-2400 can increase vascular perfusion and reduce hypoxia in murine BC, resulting in synergistic therapeutic effectiveness of DX-2400 combined with radiation. We also found that iNOS appears to mediate these beneficial effects of MMP14 blockade in combination with radiation.

Inhibition of MMP14 has antiangiogenic effects when examined at late stages of tumor development (9,10). However, we show that vascular responses differ at earlier time points. Our findings demonstrate improved vascular function at day 4 following MMP14 inhibition that seems to be achieved through a reduction in vessel tortuosity and an increase in vessel diameter. We confirmed previous findings that antibody inhibition of MMP14 can slow primary tumor growth (9,10), suggesting that an antiangiogenic response is not required for the initial growth retardation from MMP14 inhibition, although it may contribute at later stages.

Typically, tumor-associated macrophages are polarized towards an M2-like state and provide support for tumor growth and progression (27,39). Consistent with the decrease in TGFβ, we discovered that DX-2400 induced M1-like macrophages that could contribute to primary tumor growth delay. We found that proliferation was reduced and necrosis increased. Activated NK cells can control tumor growth by inhibiting cellular proliferation and promoting apoptosis (40,41). TGFβ produced in the tumor stroma, however, leads to impaired NK cell function (40,42). In concordance with the reduction in TGFβ following DX-2400 treatment, we showed an increase in NK cells and granzyme B production with DX-2400.

The DX-2400–associated increase in iNOS at day 4 allied with an increase in vessel perfusion and a reduction in tumor hypoxia in the 4T1 model. Further, iNOS blockade prevented these vascular changes and resulted in the loss of synergy in combination with radiation. In the E0771 model, while macrophage numbers and macrophage-associated iNOS increased, tumor-wide iNOS expression and hypoxia were not substantially affected. This difference in response to DX-2400 is consistent with the failure of combination therapy to result in a more than additive benefit in the E0771 model but may also reflect differences in the power to assess these differences because of the reduced sample size of E0771 compared with the study using 4T1 tumors. The sample sizes chosen were based on tumor growth curves from earlier studies using these models and a preliminary study using DX-2400, but the strength of our conclusions would have benefited from additional animals at early time points in the 4T1 model and in studies using E0771 tumors. Biologically, 4T1 and E0771 tumors differ in several respects, including endogenous MMP14 and iNOS expression, and altered response to DX-2400 could also reflect a combination of these differences. Moreover, the control tumors also differ considerably in their microvascular densities (Supplementary Figure 12, available online). Extravascular components are also important indirect regulators of vessel perfusion in solid tumors (43–45). Reduction in solid stress, such as by tumor cell death, could open nonfunctional vessels and markedly increase tumor perfusion (44). Another potential mechanism by which DX-2400 could increase

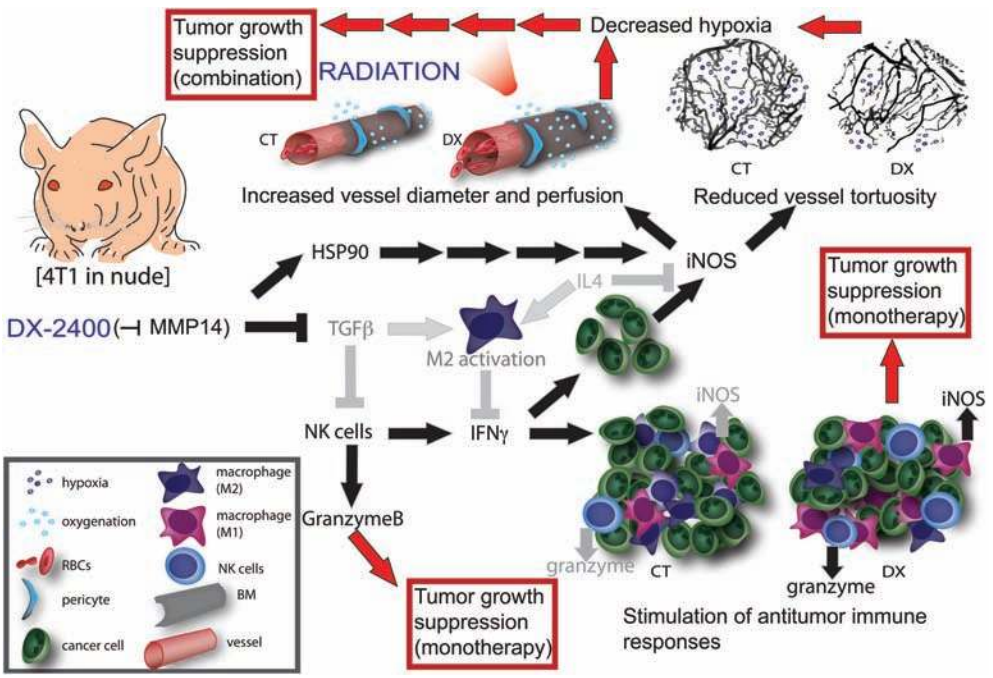

Figure 7. A schematic representation of the effects of MMP14 inhibition by DX-2400 in 4T1 primary breast tumors in nude mice. Pathways in **gray** are decreased by DX-2400 and those in **black** are increased. **Red arrows** show potential implications for monotherapy and combination therapies. DX-2400 increases vessel perfusion and tumor oxygenation; this is associated with an increase in iNOS expression in the tumor and coincides with an increase in HSP90. DX-2400 treatment also decreased vessel tortuosity, which possibly contributes to improved vessel perfusion. Improved perfusion led to an increase in the efficacy of radiation therapy. DX-2400 reduces TGFβ as well as M2-associated cytokine IL4 and the M2 marker MRC1, while it increases IFNγ, granzyme B, and iNOS—all markers of antitumor immune activity. A shift towards antitumor immune activity could contribute to the tumor growth delay seen earlier than the previously documented antiangiogenic effects. BM = basement membrane; CT = control; DX = DX-2400; NK = natural killer; RBC = red blood cell.

tissue oxygenation is through decreased oxygen consumption by cancer cells, an effect that iNOS could also mediate (46).

Although radiation therapy is not widely used in the neoadjuvant setting for BC, we utilized it here for two reasons: 1) to evaluate the potential usefulness of MMP14 inhibition in other tumors for which radiation is more commonly utilized, and 2) to use radiation as an additional tool to evaluate DX-2400–induced changes in tumor oxygenation. The data obtained fulfill both purposes. The synergistic tumor growth delay achieved in the 4T1 model was modest, however. This is consistent with the relatively low average hypoxic fraction in control 4T1 tumors, approximatley 20% at day 4 by CA9 staining fraction. Given that a dose of 6 Gy of irradiation can kill approximately 70% of oxygenated 4T1 clonogenic cells in vitro (47), each 6 Gy fraction used here would only eliminate aproximately 55% to 60% of all clonogenic 4T1 cells, and so even converting all hypoxic cells to oxygenated cells before irradiation would only decrease the survival fraction by a further 10% to 15%. Higher doses of radiation per fraction and/or lower tumor oxygenation (ie, more hypoxic tumors) might be expected to result in greater synergy.

Inhibition of MMP14 slowed growth of BC in orthotopic murine models and improved their response to concurrent radiation therapy via improved tissue oxygenation (Figure 7). We found a novel association between antibody inhibition of MMP14 and an antitumor shift in macrophages and tumor immunity that could contribute to tumor growth delay resulting from anti-MMP14 monotherapy. Moreover, the increase in MMP14 blockade–induced tumor iNOS led to improved vascular function and tissue oxygenation resulting in enhanced radiation response. These findings suggest MMP14 as a potential therapeutic target to modulate the tumor microenvironment and iNOS induction as a potential biomarker.

Funding

This work was supported in part by the US Department of Defense (DoD) Breast Cancer Research Innovator Award W81XWH-10-1-0016 (RKJ); US National Cancer Institute (NCI) grants R01-CA126642 (RKJ), P01-CA080124 (RKJ and DF), R01-CA096915, and S10-RR027070 (DF); P30-CA06516 (DMF and (AM); NCI/Federal Share Proton Beam Program Income (RKJ); DYAX Corporation (RKJ); DoD Research Fellowship W81XWH-11-1-0619 (YH); Australian-American Fulbright Association Fellowship and American Society of Clinical Oncology Young Investigator Award (SG); Italian Association for Cancer Research (AIRC) Postdoctoral Fellowship (13604) and Susan G. Komen Postdoctoral Fellowship (PDF14301739) (GS); Paul Calabresi Career Development Award in Clinical Oncology 2K12CA090354-11 (MS); and Deutsche Forschungsgemeinschaft (DFG) Fellowship AS 422/2-1 (VA).

Notes

We thank Julia Kahn (MFP window implantation), Vikash Pal Singh Chauhan (OFDI instruction), Carolyn Smith (PCNA and Apoptag staining and frozen sectioning), and Anna Khachatryan (TGFβ levels in vitro).

The authors have no conflicts of interest to declare.

References

1. Kessenbrock K, Plaks V, Werb Z. Matrix metalloproteinases: regulators of the tumor microenvironment. *Cell*. 2010;141(1):52–67.
2. Tetu B, Brisson J, Wang CS, et al. The influence of MMP-14, TIMP-2 and MMP-2 expression on breast cancer prognosis. *Breast Cancer Res*. 2006;8(3):R28.
3. Jiang WG, Davies G, Martin TA, et al. Expression of membrane type-1 matrix metalloproteinase, MT1-MMP in human breast cancer and its impact on invasiveness of breast cancer cells. *Int J Mol Med*. 2006;17(4):583–590.
4. Coussens LM, Fingleton B, Matrisian LM. Matrix metalloproteinase inhibitors and cancer: trials and tribulations. *Science*. 2002;295(5564):2387–2392.
5. Pavlaki M, Zucker S. Matrix metalloproteinase inhibitors (MMPIs): the beginning of phase I or the termination of phase III clinical trials. *Cancer Metastasis Rev*. 2003;22(2–3):177–203.
6. Glasspool RM, Twelves CJ. Matrix metalloproteinase inhibitors: past lessons and future prospects in breast cancer. *Breast*. 2001;10(5):368–378.
7. Hidalgo M, Eckhardt SG. Development of matrix metalloproteinase inhibitors in cancer therapy. *J Natl Cancer Inst*. 2001;93(3):178–193.
8. Perentes JY, Kirkpatrick ND, Nagano S, et al. Cancer Cell-Associated MT1-MMP Promotes Blood Vessel Invasion and Distant Metastasis in Triple-Negative Mammary Tumors. *Cancer Res*. 2011;71(13):4527–4538.
9. Devy L, Huang L, Naa L, et al. Selective inhibition of matrix metalloproteinase-14 blocks tumor growth, invasion, and angiogenesis. *Cancer Res*. 2009;69(4):1517–1526.
10. Kaimal R, Aljumaily R, Tressel SL, et al. Selective blockade of matrix metalloprotease-14 with a monoclonal antibody abrogates invasion, angiogenesis and tumor growth in ovarian cancer. *Cancer Res*. 2013;73(8):2457–2467.
11. Alfranca A, Lopez-Oliva JM, Genis L, et al. PGE2 induces angiogenesis via MT1-MMP-mediated activation of the TGFbeta/Alk5 signaling pathway. *Blood*. 2008;112(4):1120–1128.
12. Carmeliet P, Jain RK. Molecular mechanisms and clinical applications of angiogenesis. *Nature*. 2011;473(7347):298–307.
13. Cheng G, Liao S, Kit Wong H, et al. Engineered blood vessel networks connect to host vasculature via wrapping-and-tapping anastomosis. *Blood*. 2011;118(17):4740–4749.
14. Goel S, Duda DG, Xu L, et al. Normalization of the vasculature for treatment of cancer and other diseases. *Physiol Rev*. 2011;91(3):1071–1121.
15. Carmeliet P, Jain RK. Principles and mechanisms of vessel normalization for cancer and other angiogenic diseases. *Nat Rev Drug Discov*. 2011;10(6):417–427.
16. Winkler F, Kozin SV, Tong RT, et al. Kinetics of vascular normalization by VEGFR2 blockade governs brain tumor response to radiation: role of oxygenation, angiopoietin-1, and matrix metalloproteinases. *Cancer Cell*. 2004;6(6):553–563.
17. Richardsen E, Uglehus RD, Johnsen SH, Busund LT. Immunohistochemical expression of epithelial and stromal immunomodulatory signalling molecules is a prognostic indicator in breast cancer. *BMC Res Notes*. 2012;5:110.
18. Sounni NE, Dehne K, van Kempen L, et al. Stromal regulation of vessel stability by MMP14 and TGFbeta. *Dis Model Mech*. 2010;3(5–6):317–332.
19. van Meeteren LA, Goumans MJ, ten Dijke P. TGF-beta receptor signaling pathways in angiogenesis; emerging targets for anti-angiogenesis therapy. *Curr Pharm Biotechnol*. 2011;12(12):2108–2120.
20. Liu J, Liao S, Diop-Frimpong B, et al. TGF-beta blockade improves the distribution and efficacy of therapeutics in breast carcinoma by normalizing the tumor stroma. *Proc Natl Acad Sci U S A*. 2012;109(41):16618–16623.
21. Fridlender ZG, Sun J, Kim S, et al. Polarization of tumor-associated neutrophil phenotype by TGF-beta: "N1" versus "N2" TAN. *Cancer Cell*. 2009;16(3):183–194.
22. Krstic J, Santibanez JF. Transforming growth factor-beta and matrix metalloproteinases: functional interactions in tumor stroma-infiltrating myeloid cells. *Scientific World J*. 2014;2014:521754.
23. Luo H, Hao Y, Tang B, Zeng D, Shi Y, Yu P. Mouse forestomach carcinoma cells immunosuppress macrophages through transforming growth factor-beta1. *Mol Med Rep*. 2012;5(4):988–992.
24. Wu A, Wei J, Kong LY, et al. Glioma cancer stem cells induce immunosuppressive macrophages/microglia. *Neuro Oncol*. 2010;12(11):1113–1125.
25. Wrzesinski SH, Wan YY, Flavell RA. Transforming growth factor-beta and the immune response: implications for anticancer therapy. *Clin Cancer Res*. 2007;13(18 Pt 1):5262–5270.
26. Wojtowicz-Praga S. Reversal of tumor-induced immunosuppression by TGF-beta inhibitors. *Invest New Drugs*. 2003;21(1):21–32.
27. Hao NB, Lu MH, Fan YH, Cao YL, Zhang ZR, Yang SM. Macrophages in tumor microenvironments and the progression of tumors. *Clin Dev Immunol*. 2012;2012:948098.
28. Vakoc BJ, Lanning RM, Tyrrell JA, et al. Three-dimensional microscopy of the tumor microenvironment in vivo using optical frequency domain imaging. *Nat Med*. 2009;15(10):1219–1223.
29. Schneider CA, Rasband WS, Eliceiri KW. NIH Image to ImageJ: 25 years of image analysis. *Nat Methods*. 2012;9(7):671–675.
30. Nagareddy PR, Rajput PS, Vasudevan H, et al. Inhibition of matrix metalloproteinase-2 improves endothelial function and prevents hypertension in insulin-resistant rats. *Br J Pharmacol*. 2012;165(3):705–715.
31. Butler GS, Dean RA, Tam EM, Overall CM. Pharmacoproteomics of a metalloproteinase hydroxamate inhibitor in breast cancer cells: dynamics of membrane type 1 matrix metalloproteinase-mediated membrane protein shedding. *Mol Cell Biol*. 2008;28(15):4896–4914.
32. Luo S, Wang T, Qin H, Lei H, Xia Y. Obligatory role of heat shock protein 90 in iNOS induction. *Am J Physiol Cell Physiol*. 2011;301(1):C227–C233.

33. Perfetto B, Buommino E, Canozo N, et al. Interferon-gamma cooperates with Helicobacter pylori to induce iNOS-related apoptosis in AGS gastric adenocarcinoma cells. *Res Microbiol*. 2004;155(4):259–266.
34. Garban HJ, Bonavida B. Nitric oxide sensitizes ovarian tumor cells to Fas-induced apoptosis. *Gynecol Oncol*. 1999;73(2):257–264.
35. Berra A, Ganzinelli S, Saravia M, Borda E, Sterin-Borda L. Inducible nitric oxide synthase subserves cholinergic vasodilation in retina. *Vis Neurosci*. 2005;22(3):371–377.
36. Bustamante SA, Pang Y, Romero S, et al. Inducible nitric oxide synthase and the regulation of central vessel caliber in the fetal rat. *Circulation*. 1996;94(8):1948–1953.
37. Huang Y, Stylianopoulos T, Duda DG, Fukumura D, Jain RK. Benefits of vascular normalization are dose and time dependent--letter. *Cancer Res*. 2013;73(23):7144–7146.
38. Fukumura D, Kashiwagi S, Jain RK. The role of nitric oxide in tumour progression. *Nat Rev Cancer*. 2006;6(7):521–534.
39. Rai RK, Vishvakarma NK, Mohapatra TM, Singh SM. Augmented macrophage differentiation and polarization of tumor-associated macrophages towards M1 subtype in listeria-administered tumor-bearing host. *J Immunother*. 2012;35(7):544–554.
40. Mamessier E, Sylvain A, Thibult ML, et al. Human breast cancer cells enhance self tolerance by promoting evasion from NK cell antitumor immunity. *J Clin Invest*. 2011;121(9):3609–3622.
41. Ascierto ML, Idowu MO, Zhao Y, et al. Molecular signatures mostly associated with NK cells are predictive of relapse free survival in breast cancer patients. *J Transl Med*. 2013;11(1):145.
42. Bruno A, Focaccetti C, Pagani A, et al. The proangiogenic phenotype of natural killer cells in patients with non-small cell lung cancer. *Neoplasia*. 2013;15(2):133–142.
43. Stylianopoulos T, Martin JD, Chauhan VP, et al. Causes, consequences, and remedies for growth-induced solid stress in murine and human tumors. *Proc Natl Acad Sci U S A*. 2012;109(38):15101–15108.
44. Stylianopoulos T, Jain RK. Combining two strategies to improve perfusion and drug delivery in solid tumors. *Proc Natl Acad Sci U S A*. 2013;110(46):18632–18637.
45. Chauhan VP, Martin JD, Liu H, et al. Angiotensin inhibition enhances drug delivery and potentiates chemotherapy by decompressing tumour blood vessels. *Nat Commun*. 2013;4:2516.
46. Jiang H, De Ridder M, Verovski VN, et al. Activated macrophages as a novel determinant of tumor cell radioresponse: the role of nitric oxide-mediated inhibition of cellular respiration and oxygen sparing. *Int J Radiat Oncol Biol Phys*. 2010;76(5):1520–1527.
47. Bouquet F, Pal A, Pilones KA, et al. TGFbeta1 inhibition increases the radiosensitivity of breast cancer cells in vitro and promotes tumor control by radiation in vivo. *Clin Cancer Res*. 2011;17(21):6754–6765.